CHAPTER 3

THE PROPOSED ROBUST FIELD WEAKENING CONTROL STRATEGY FOR SMPMSM DRIVES

3.1 Introduction

As described in the previous chapter, some benefits can be obtained from the control strategy of $i_{ds} = 0$, but the operating speed range will be quite restricted. In order to effectively extend the operating speed range, many field weakening control methods were proposed [4,8,10-14]. Some field weakening control methods [4,8,10,11] calculate the desired current commands based on the accurate model parameters to achieve fast dynamic response and/or better efficiency. However, the resulting performance will deteriorate when the model parameters are varied with different operating conditions. Hence, to overcome this disadvantage, several robust field weakening controls were proposed to achieve a robust drive [12-14]. The field weakening control method proposed by [12] may result in unstable operation of the drive system. Another method [13] is proposed by adjusting the d-axis current command as well as the upper/lower bounds of the maximum q-axis current of the speed controller through a proportional-integral (PI) [13] or integral (I) [14,17,18] controller of the error between the maximum inverter output voltage and the output voltage resulting from the PI current controllers. However, it is found that the corresponding q-axis current bounds under transient condition can not follow the true bounds instantaneously. In these methods, either a PI controller or an integral controller is used to adjust gradually the d- and q-axes current commands to the correct operating point. This convergent rate through the feedback (either PI or I) control may be very slow or even unstable for a large abrupt demand torque change.

In view of above discussions, to fully exploit the available torque capability and to achieve the minimum copper loss in spite of the variations of the parameters of the SMPMSM drives become the major motivation of this chapter.

In this chapter, the extension of the speed operation range is made by using the field weakening control strategy such that the SMPMSM drive can be operated over wider speed range than that of $i_{ds} = 0$ control strategy. First, a novel field weakening control based on a beautiful closed form solution of the available maximum torque is proposed to eliminate the gradual adjustment by feedback mechanism so as to achieve faster response and better stability. Next, the proposed robust field weakening control strategy is described in detail. Finally, some simulation and experimental results resulting from a DSP-based prototype drive are given to verify the validity of the proposed strategy.

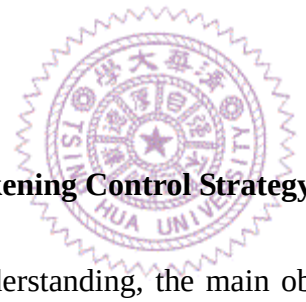

3.2 The Proposed Field Weakening Control Strategy for SMPMSM Drives

Based on the previous understanding, the main objective is to propose a robust controller to achieve both fast dynamic response and minimum copper loss for the whole operating region. First, as far as the first and the fourth regions are concerned, since the maximum torque T_{eM1} and T_{eN1} are constant and are limited only by I_{sm}, hence whenever an accelerating or braking torque is required, the corresponding maximum torque can be applied to achieve the fastest response. Also, in these two non-field-weakening regions, $i_{ds} = 0$, the maximum torque per ampere control (or minimum copper loss control) is automatically achieved by the closed loop speed controller without the influence of the parameter changes. For other three regions, the corresponding maximum torques T_{eM2}, T_{eM3} and T_{eN2} are speed dependent. Instead of using an integral control to approach gradually the available maximum torque, a

real-time computation method is proposed to calculate directly the maximum accelerating and braking torque-producing currents, namely $I_{qs\max}$ and $I_{qs\min}$, at this speed. Therefore, under transient condition, one can immediately apply the maximum torque to achieve the fastest response. Of course, under steady state, the resulting T_e will be equal to the loading torque through the speed loop control. Thus, considering the practical implementation problem as well as to achieve minimum copper loss, the robust control strategy is proposed as shown in Fig. 3.1. From Fig. 3.1, one can see that except the PI speed controller with variable-bounds antiwindup, the upper and lower (U/L) I_{qs} bounds calculator, the minimum copper loss controller (namely MCL controller) and the robust tuner. The detailed description for the speed control system shown in Fig 3.1 will be explained in the section 3.4.

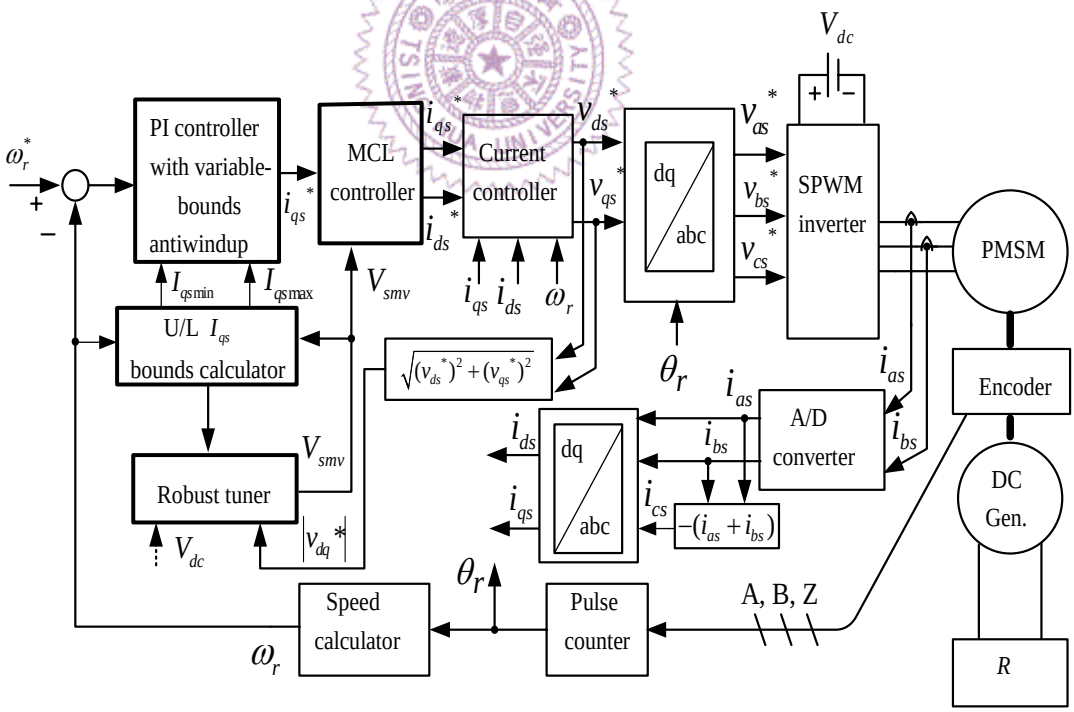

Fig. 3.1. Block diagram of the speed control system of the SMPMSM drive

A. The Proposed Real Time Calculator for the Upper and Lower I_{qs} Bounds

As can be observed from the previous chapter, there are five regions for positive ω_r speed and other five regions for negative ω_r speed. In order to simplify the implementation, no region detector is adopted to identify the operating regions. Instead, a real-time upper and lower q-axis current bounds (namely $I_{qs\max}$ and $I_{qs\min}$) calculator is proposed for convenient integration of the novel robust controller. First, from (2.8) and (2.10) the corresponding current and voltage bounds trajectories can be expressed as follows:

$$f_1(i_{ds}, i_{qs}) = {i_{ds}}^2 + {i_{qs}}^2 - {I_{sm}}^2 = 0 \tag{3.1}$$

$$f_2(i_{ds}, i_{qs}, \omega_e, V_{sm}) = (i_{ds} - i_{dc})^2 + (i_{qs} - i_{qc})^2 - \frac{{V_{sm}}^2}{{R_s}^2 + {\omega_e}^2 {L_s}^2} = 0 \tag{3.2}$$

where i_{dc} and i_{qc} represent the coordinates of the center of the circle defined as follows:

$$i_{dc} \equiv \frac{-\omega_e{}^2 L_s \lambda_f}{{R_s}^2 + {\omega_e}^2 {L_s}^2} \quad ; \quad i_{qc} \equiv \frac{-\omega_e R_s \lambda_f}{{R_s}^2 + {\omega_e}^2 {L_s}^2}$$

As can be observed from Fig. 2.2, instead of using an integral controller to gradually approach the current operating point, direct calculation of the available maximum torque during field weakening operation regions, which correspond to the intersecting points of two circles, is in fact possible.

Thus, from equation (3.1) one can get

$$i_{qs} = S\sqrt{{I_{sm}}^2 - {i_{ds}}^2} \tag{3.3}$$

Where S is an integer variable representing either +1 or -1

Substituting (3.3) into (3.2) yields the following quadratic equation of i_{ds}:

$$a{i_{ds}}^2 + b i_{ds} + c = 0 \tag{3.4}$$

where

$$a \equiv 4({i_{dc}}^2 + {i_{qc}}^2)$$

$$b \equiv 4 i_{dc}[\frac{{V_{sm}}^2}{{R_s}^2 + {\omega_e}^2 {L_s}^2} - ({I_{sm}}^2 + {i_{dc}}^2 + {i_{qc}}^2)]$$

$$c \equiv [({I_{sm}}^2 + {i_{dc}}^2 + {i_{qc}}^2) - (\frac{{V_{sm}}^2}{{R_s}^2 + {\omega_e}^2 {L_s}^2})]^2 - 4{i_{qc}}^2 {I_{sm}}^2$$

It follows from (3.4) that one can get the following closed form solutions:

$$i_{d1} \equiv \frac{-b - \sqrt{b^2 - 4ac}}{2a} \tag{3.5}$$

$$i_{d2} \equiv \frac{-b + \sqrt{b^2 - 4ac}}{2a} \tag{3.6}$$

As mentioned before, the feasible solution region of the drive system corresponds to the region satisfied by both (2.8) and (2.10). As an illustration, consider Fig. 2.2(a) for ω_{r1} speed, the feasible region corresponds to the region enclosed by the closed curve BHNGFMEDCB. However, as far as the practical operable region is concerned only that portion defined by BHOGFMEDCB is qualified. In other words, it is required that i_{ds} be less than or equal to zero. In view of the above considerations, the proposed real-time upper/lower I_{qs} bounds calculator for positive speed may be summarized as follows:

Step1. Calculate $b^2 - 4ac$ and check if $b^2 - 4ac \le 0$.

If yes, then the corresponding available maximum and minimum torques are

$$T_{e\max} = T_{eM1}$$

$$T_{e\min} = T_{eN1}$$

For convenience, the corresponding upper and lower d-axis and q-axis current bounds (i_{du}, i_{qu} and i_{dl}, i_{ql}) are represented as follows:

$$(i_{du}, i_{qu}) = (0, I_{sm})$$

$$(i_{dl}, i_{ql}) = (0, -I_{sm})$$

Step2. If $b^2 - 4ac > 0$, then calculate i_{d1} and i_{d2} as per (3.5) and (3.6)

Step3. Check if $i_{d1} \geq 0$?

If $i_{d1} \geq 0$, then let

$$(i_{du}, i_{qu}) = (0, I_{sm}), \quad T_{e\max} = T_{eM1}$$

Otherwise, let

$$(i_{du}, i_{qu}) = (i_{d1}, \sqrt{I_{sm}^{\ 2} - i_{d1}^{\ 2}}), \quad T_{e\max} = T_{eM2} \quad \text{or} \quad T_{eM3}$$

Step4. Check if $i_{d2} \geq 0$?

If $i_{d2} \geq 0$, then let

$$(i_{dl}, i_{ql}) = (0, -I_{sm}), \quad T_{e\min} = T_{eN1}$$

Otherwise, let

$$(i_{dl}, i_{ql}) = (i_{d2}, -\sqrt{I_{sm}^{\ 2} - i_{d2}^{\ 2}}), \quad T_{e\min} = T_{eN2}$$

Step5. The corresponding upper and lower I_{qs} bounds are given as

$$I_{qs\max} = i_{qu}, \text{ for } \omega_r > 0$$

$$I_{qs\min} = i_{ql}, \text{ for } \omega_r > 0$$

It should be pointed out here that in step 1 to avoid dividing zero, this real time calculator is initiated for $|\omega_r| > 0$. Also, from the symmetric property between the first (fourth) quadrant and the third (second) quadrant on the torque vs. speed plane, one can modify the above procedure easily for negative ω_r speed operation. In other words, if $\omega_r < 0$, then one can take its absolute value, namely $|\omega_r|$ and proceed

from step 1 to step 4. Then the corresponding $I_{qs\max}$ and $I_{qs\min}$ in step 5 take the following forms:

$$I_{qs\max} = -i_{ql}, \text{ for } \omega_r < 0$$

$$I_{qs\min} = -i_{qu}, \text{ for } \omega_r < 0$$

It is seen from the above description of the proposed calculator that the computation cost of (3.5) and (3.6) is quite limited and can be realized in real time easily. Also, since the maximum I_{qs}, which corresponds to the maximum torque, is always available, it follows that as soon as a transient state is initiated, one can immediately apply the maximum torque to achieve the fastest response. It is no longer required to wait for some time until the integral control reaches the steady state to achieve the correct answer.

Finally, for convenient integration of the proposed controller, an indicator, namely Z, is proposed for showing the field weakening status as follows:

$$Z \equiv sign(i_{du}) = \begin{cases} 1, & for \quad i_{du} < 0 \\ 0, & for \quad i_{du} \geq 0 \end{cases}$$

It is also worth mentioning here that the above real time upper and lower bounds are calculated based on the nominal parameters. As such, a robust tuner as will be seen later is used to get the fine tuning.

B. The PI Controller with Variable-Bounds Antiwindup

From Fig. 3.1 one can see that the proposed robust controller also adopts a conventional PI controller as the speed controller. Similarly, to avoid the saturation problems which may lead to significant deterioration of performance of a PI speed controller, an antiwindup method [59] as shown in Fig. 2.5 is adapted. In other words, instead of using a fixed upper/lower bounds like [59], actual upper and lower I_{qs}

bounds of the proposed speed controller are updated in real time to achieve fast response as well as automatic field-weakening control.

C. The Robust Tuner and the Minimum Copper Loss Controller

As mentioned before, for regions one and four, the forward maximum torque and the maximum braking torque are constant and independent of the parameter variations. In addition, the closed loop speed control will adjust the torque to match the load torque automatically. In summary, in the non-field-weakening regions, one can achieve i_{qs}^{*} and zero i_{ds}^{*} robustly and with minimum copper loss (or maximum torque per ampere control). However, when the parameters such as $R_s, L_s, \lambda_f, V_{sm}$ are varied, then the corresponding functional value of f_2 in (3.2) will also be modified. As a result, the resulting d-axis and q-axis stator current commands will not be correct and may degrade the dynamic response and efficiency. Hence, a fine tuner, called the robust tuner in Fig. 3.1, is added to cope with the parameter changes. The proposed robust tuner will then make proper corrections in field weakening control regions and when the operating point is not with minimum copper loss. Also, to achieve minimum copper loss, the maximum output phase voltage magnitude (V_{sm}) of the inverter must be applied to the SMPMSM during field weakening control region [14].

Next, after careful examination of (3.2) shows that in case parameters R_s, L_s and λ_f are changed at a given speed and for the same i_{ds} and i_{qs} values, then the corresponding V_{sm} should also be changed such that the equality remains valid.

In view of the above thinking, a virtual maximum stator phase voltage amplitude (V_{smv}) is proposed as follows:

$$V_{smv} = V_{sm} + K_I \int_0^t Z(V_{cm} - |v_{dq}^{*}|)dt \tag{3.7}$$

where K_I denotes the integral gain, V_{cm} is the peak value of the triangular carrier signal of the sinusoidal pulse-width modulated (SPWM) inverter and $\left|v_{dq}^{*}\right| = \sqrt{(v_{ds}^{*})^2 + (v_{qs}^{*})^2}$; v_{ds}^{*} and v_{qs}^{*} denote the output voltage commands of the d-axis and q-axis current controller respectively.

Since V_{sm} is obtained from the DC link voltage ($V_{sm} = \frac{V_{dc}}{2}$ for SPWM strategy), addition of a V_{dc} sensor may result in increasing cost and deteriorate the robust structure. However, for electrical vehicle applications, the variation of V_{dc} may be quite significant. Thus, another sensorless approach may be given as follows:

$$V_{smv} = V_{sm0} + K_I \int_0^t Z(V_{cm} - \left|v_{dq}^{*}\right|)dt \tag{3.8}$$

where V_{sm0} denotes the nominal maximum output phase voltage amplitude of the inverter. In other words, the corresponding correct V_{smv} can still be achieved through the integral feedback adjustment.

Once the total effect of the parameter variations is lumped together in the virtual V_{sm}, it is now quite simple to achieve robust control and minimum copper loss in the field weakening region. First, the correct $I_{qs\max}$ and $I_{qs\min}$ is corrected by replacing V_{sm} with V_{smv} in the U/L I_{qs} bounds calculator with the same procedure. The resulting correct i_{qs}^{*} is then obtained automatically no matter it is under transient or steady state condition. Finally, the corresponding i_{ds}^{*} command is determined from the minimum copper loss controller in Fig. 3.1 as follows:

$$i_{ds}^{*} = i_{dc} + \sqrt{\frac{V_{smv}^{\ 2}}{R_s^{\ 2} + \omega_e^{\ 2} L_s^{\ 2}} - (i_{qs}^{*} - i_{qc})^2} \tag{3.9}$$

Depending on various operating conditions such as during braking operation or

operating in partial field weakening region, the i_{ds}^{*} obtained from (3.9) may become positive. Under this condition, one should set i_{ds}^{*} equal to zero.

From the above illustrations, it is seen that the proposed robust field weakening control can achieve not only fast dynamic response but also minimum copper loss during the whole operating range and in spite of the parameter variations. Also, due to application of the proposed real time maximum I_{qs} bounds calculator, instead of using an integral control to gradually approach the correct solution, there is no stability problem for an abrupt and large load torque change. Moreover, elimination of using a region detector greatly simplifies the implementation problem of the proposed robust controller.

3.3 Simulation Results

To facilitate understanding the proposed control strategy and also verify the validity of the proposed methods, some simulations are first provided. In this dissertation, all simulations are carried out by using the Simulink software package in Matlab. For consistency with the practical experimental setup, a permanent magnet servo DC motor is coupled to the SMPMSM whose parameters are shown in Table 2.1. The inertia coefficient and viscous damping coefficient are $7.7\times10^{-4}\ kg/m^2$ and $22\times10^{-5}\ (N\cdot m\cdot \sec/rad)$ approximately. For simplification, all power switches are considered as ideal switch. As shown in Fig 3.1, a PI speed controller with variable bounds antiwindup is set for the outer-loop speed control and two inner-loop PI current controllers are set for the d- and q-axes current control; a $10kHz$ SPWM inverter provides the desired current to the SMPMSM. Moreover, the minimum copper loss controller, upper/lower I_{qs} bounds calculator and robust tuner are all

included in the simulation program. For reference, several simulation results are provided below to show the characteristics of the proposed control strategy.

First, to demonstrate the robust characteristic of the proposed control strategy due to the variation of the dc link voltage (V_{dc}), the motor is started from rest at $t = 0$ and up to 2400 rpm with $T_L = 0$ Nm. The dc link voltage is subjected to a periodic step change of 15 V for each 1 sec and the design of the controller is based on the nominal values shown in Table 2.1. Fig. 3.2(a) shows the corresponding simulation trajectories of V_{dc}, V_{smv}, i_{ds} and i_{qs}, respectively and Fig. 3.2(b) shows the corresponding trajectories of ω_r, $|v_{dq}^*|$, i_{du} and $|i_{dq}|^2 = (i_{ds}^2 + i_{qs}^2)$ which is proportional to copper loss . From Fig. 3.2(a) one can see that V_{smv} can indeed track the variation of V_{dc} in the field weakening regions. After starting transient, the i_{qs} remains constant without the influence of the V_{dc} variations and the resulting speed is kept constant as well. As V_{smv} changes, the i_{ds} will also track the variation of V_{dc} according to (3.9) to achieve minimum copper loss. The controller can indeed achieve the objective of minimum copper loss control indeed, as observed from Figs. 3.2(a) and 3.2(b).

In the above simulations, V_{dc} is assumed to be measured directly. As a comparison, another simulation under the same conditions but without measuring V_{dc} is also repeated. The corresponding V_{smv} is obtained from (3.8) by using the feedback adjustment. From Fig. 3.3(a) one can see that the convergent rate of V_{smv} and i_{ds} becomes slower as compared with that of Fig. 3.2(a). However, the same correct results can still be obtained under steady state as can be checked from Fig. 3.3(b). In other words, one can still achieve the minimum copper loss control under the varying V_{dc} condition.

Next, consider another simulation for illustrating the robust characteristic of the proposed control strategy due to variation of parameters of the SMPMSM. The motor

is subjected a step speed command 2100 rpm with $T_L = 0$ Nm. The V_{dc} is kept at 100 V and the design of the controller is based on $R_s = 2.36\ \Omega$, $L_s = 7.4\ mH$ and $\lambda_f = 0.07237\ V/(rad/\sec)$, where $|\Delta R_s| = 33.3\%$, $|\Delta L_s| = 25\%$ and $|\Delta \lambda_f| = 25\%$, respectively, as compared to the nominal values shown in Table 2.1. In order to demonstrate the effects of the proposed robust tuner, Fig. 3.4 shows the corresponding simulated results with the robust tuner disabled ($K_I = 0$) and Fig. 3.5 shows the corresponding results with the robust tuner enabled. From Figs. 3.4(a) and 3.4(b) one can see that, under the steady state of i_{qs}, i_{ds} is less than zero but $|v_{dq}^*|$ is not equal to V_{cm}. In other words, the maximum available voltage V_{sm} is not applied and the minimum copper loss control is not achieved. In addition, as observed from Fig 3.4(a), the speed command, 2100 rpm, is not achieved. On the other hand, Fig. 3.5 shows the corresponding results with the robust tuner enabled. As shown in Figs. 3.5(a) and 3.5(b), the drive is operated in field weakening region ($i_{du} < 0$) and V_{smv} starts to tune according to (3.8). As $|v_{dq}^*|$ approaches V_{cm}, $|i_{dq}|^2$ also decreases. The drive is then operated under minimum copper loss control where $i_{ds} < 0$ and $|v_{dq}^*| = V_{cm}$. Moreover, the steady-state speed can reach the command speed, namely 2100rpm. From the above simulations, one can see that the proposed control can indeed achieve the minimum copper loss in spite of the variations of the dc link voltage and the parameters of the SMPMSM.

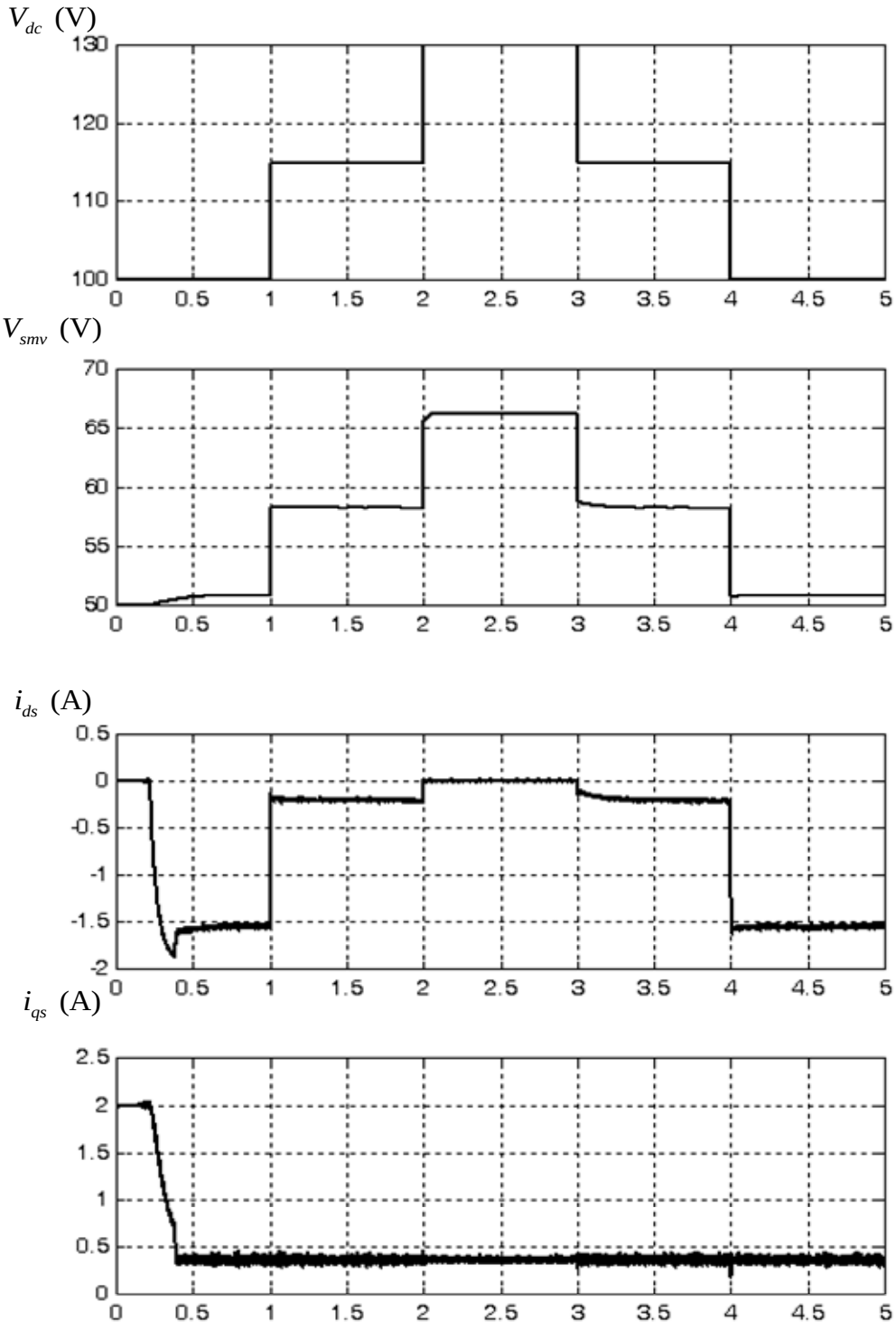

(a)

Fig. 3.2. Simulation trajectories of (a) V_{dc}, V_{smv}, i_{ds} and i_{qs}; (b) ω_r, $\left|v_{dq}^{*}\right|$, $\left|i_{dq}\right|^2$ and i_{du}, due to variation of V_{dc} and with V_{dc} sensor.

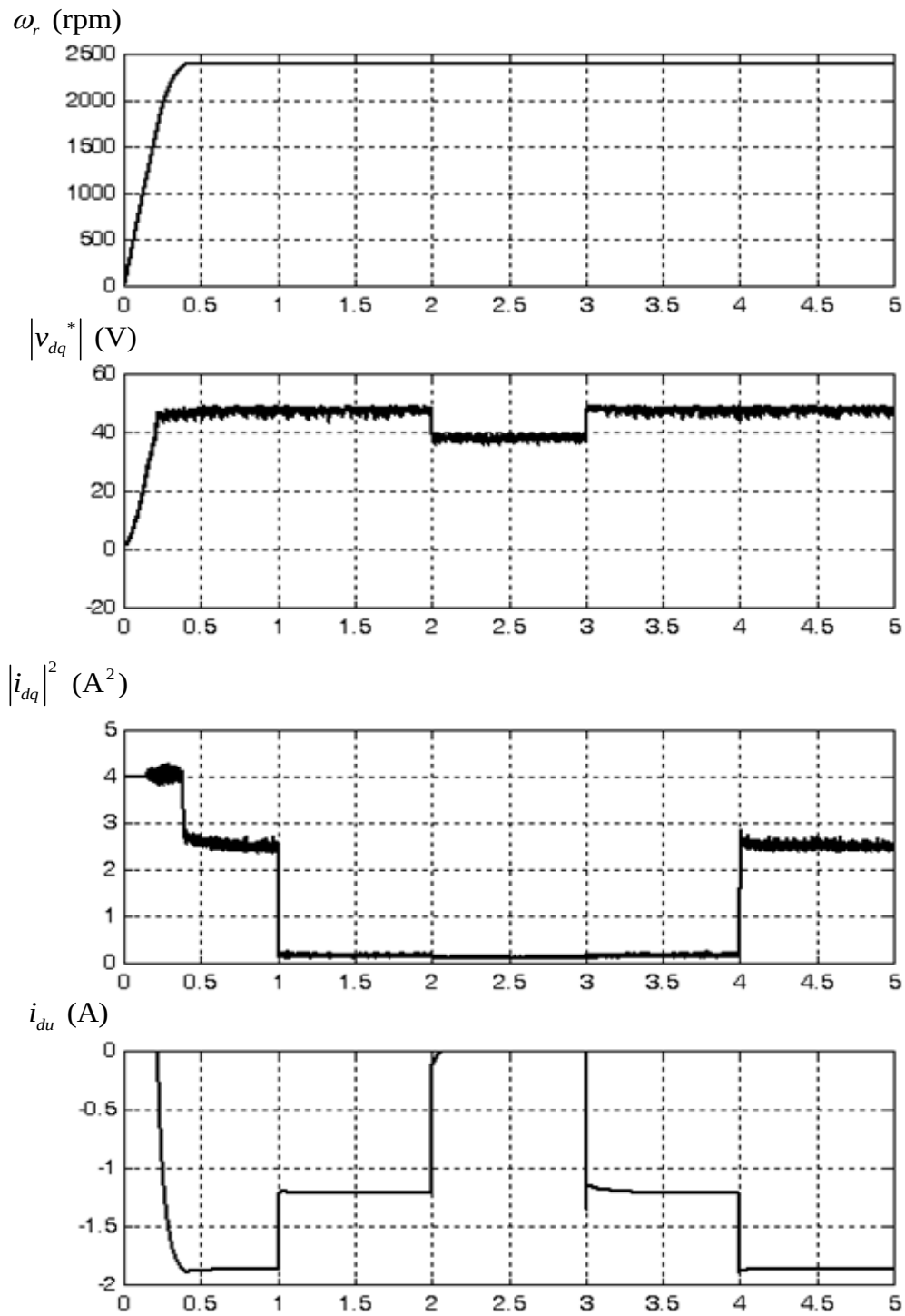

(b)

Fig. 3.2. Simulation trajectories of (a) V_{dc}, V_{smv}, i_{ds} and i_{qs}; (b) ω_r, $|v_{dq}^*|$, $|i_{dq}|^2$ and i_{du}, due to variation of V_{dc} and with V_{dc} sensor. (continued).

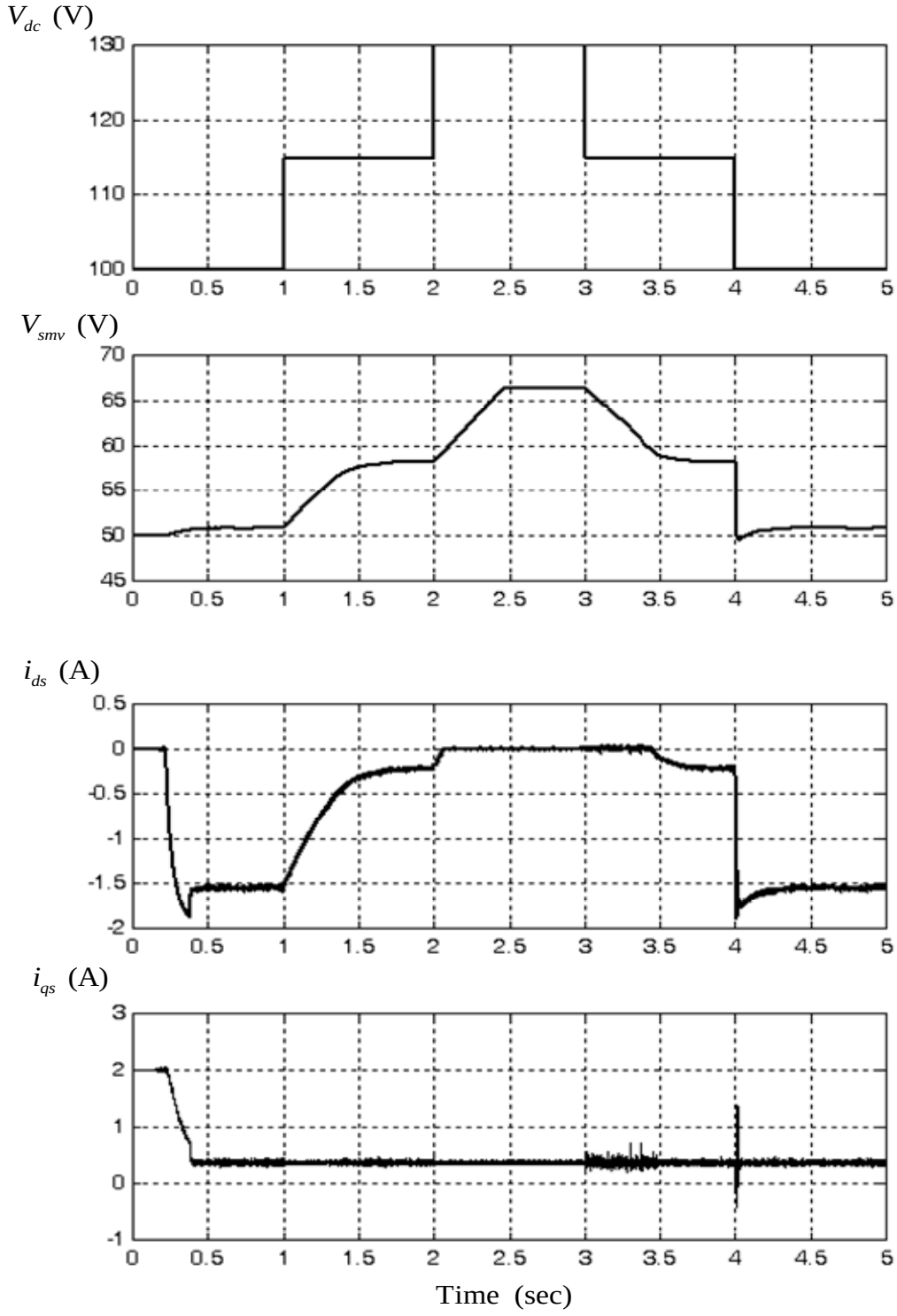

(a)

Fig. 3.3. Simulation trajectories of (a) V_{dc}, V_{smv}, i_{ds} and i_{qs}; (b) ω_r, $\left|v_{dq}^{*}\right|, \left|i_{dq}\right|^2$ and i_{du}, due to variation of V_{dc} and without V_{dc} sensor.

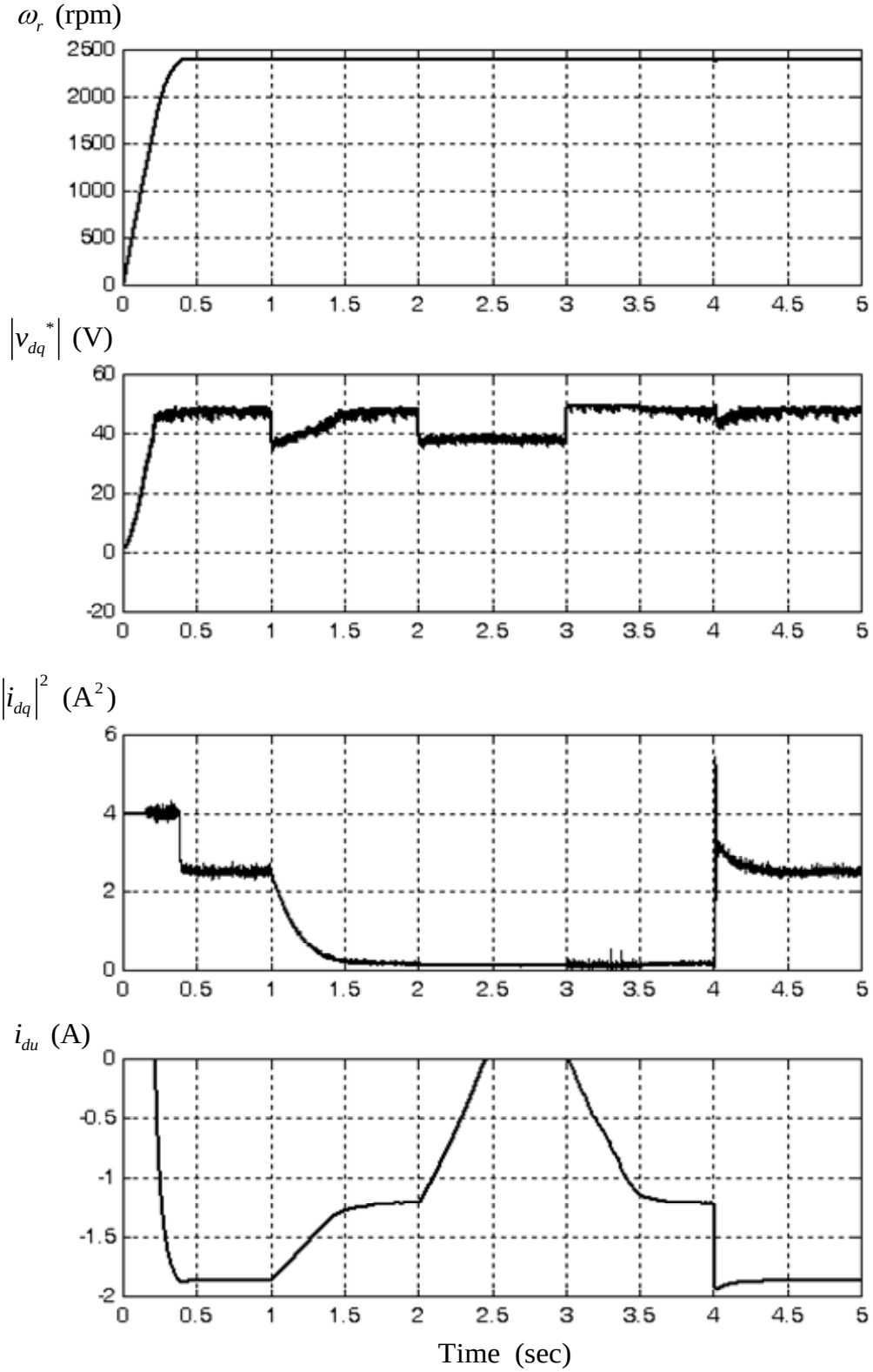

(b)

Fig. 3.3. Simulation trajectories of (a) V_{dc}, V_{smv}, i_{ds} and i_{qs}; (b) ω_r, $|v_{dq}^*|, |i_{dq}|^2$ and i_{du}, due to variation of V_{dc} and without V_{dc} sensor. (continued).

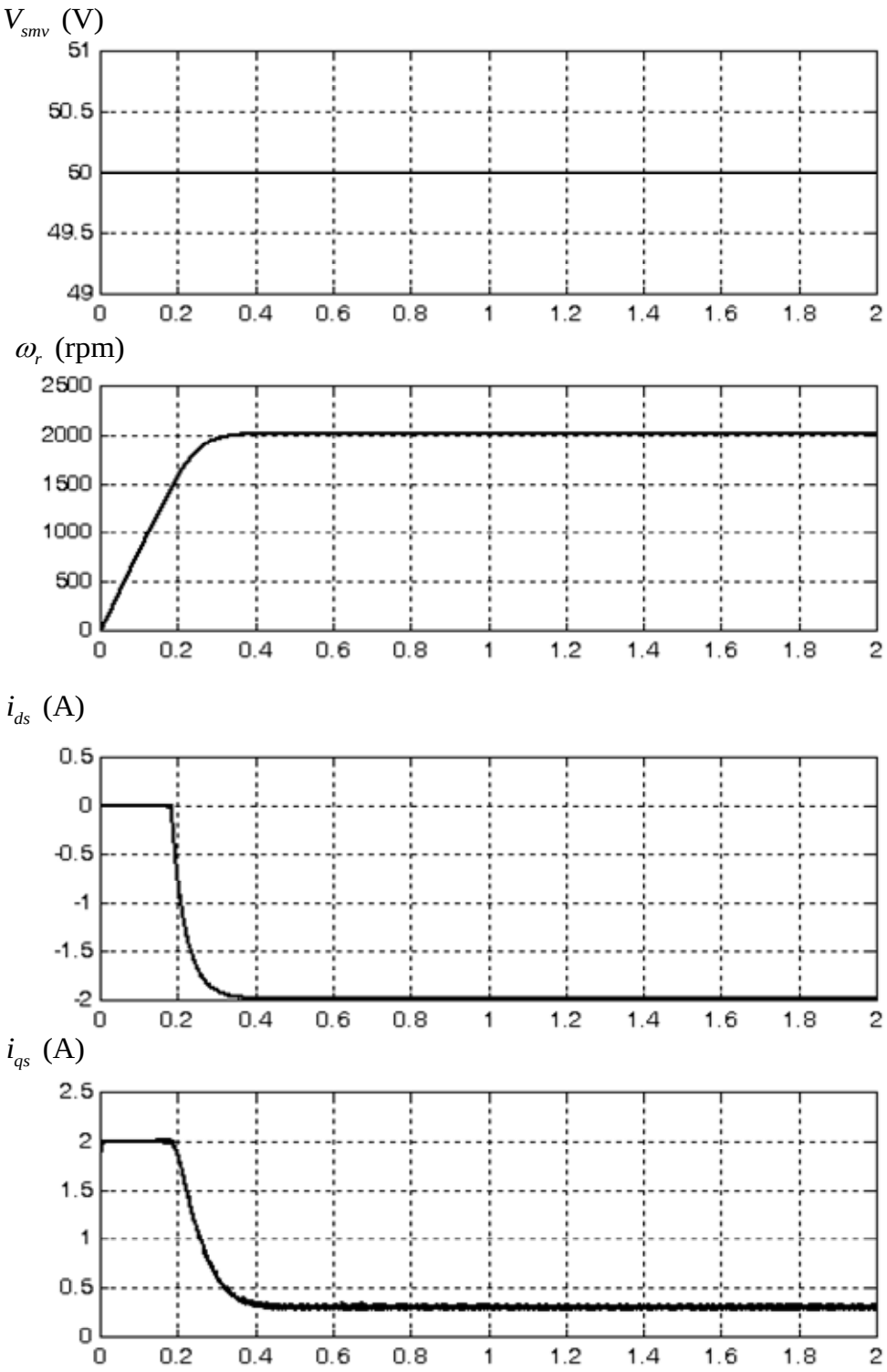

(a)

Fig. 3.4. Simulation results of (a)V_{smv}, ω_r, i_{ds} and i_{qs}; (b) $\left|v_{dq}^{*}\right|$, $\left|i_{dq}\right|^2$ and i_{du}, with the robust tuner disabled.

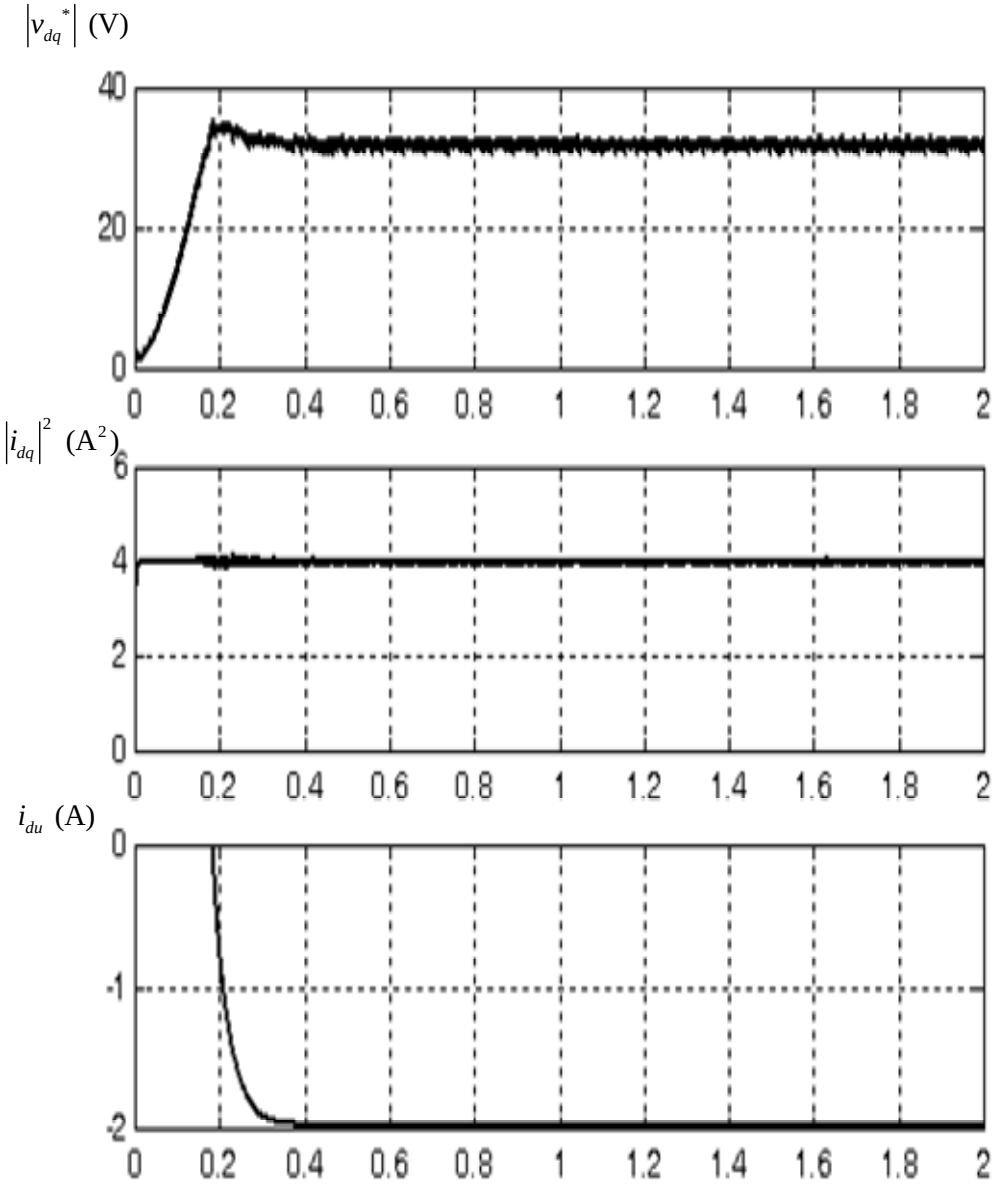

(b)

Fig. 3.4. Simulation results of (a)V_{smv}, ω_r, i_{ds} and i_{qs}; (b) $|v_{dq}^*|$, $|i_{dq}|^2$ and i_{du}, with the robust tuner disabled. (continued).

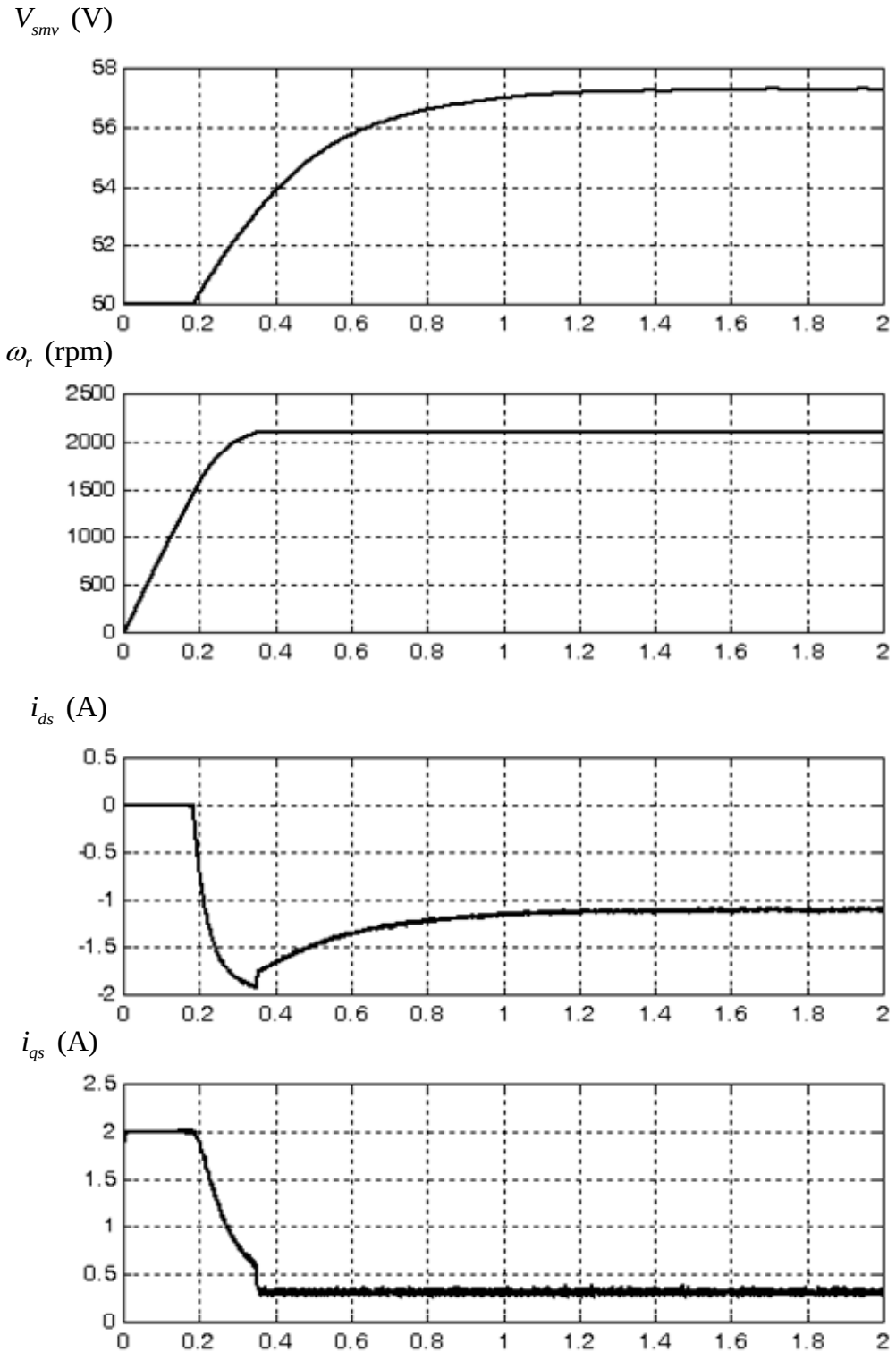

(a)

Fig. 3.5. Simulation results of (a) V_{smv}, ω_r, i_{ds} and i_{qs}; (b) $\left|v_{dq}^{*}\right|$, $\left|i_{dq}\right|^2$ and i_{du}, with the robust tuner enabled.

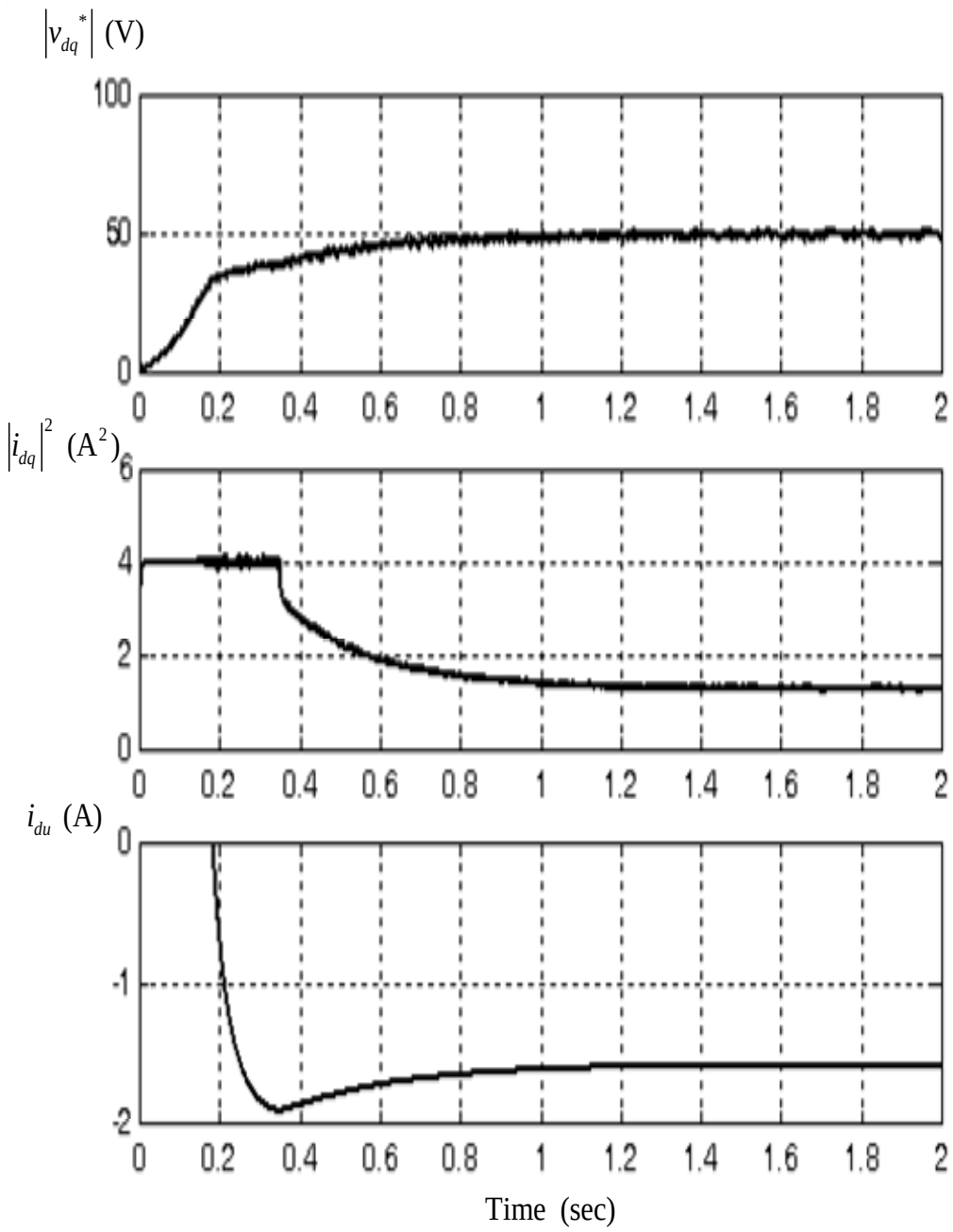

(b)

Fig. 3.5. Simulation results of (a) V_{smv}, ω_r, i_{ds} and i_{qs}; (b) $|v_{dq}^*|$, $|i_{dq}|^2$ and i_{du}, with the robust tuner enabled. (continued).

3.4 Implementation and Experimental Results

To facilitate understanding the proposed control strategy and also verify the validity of the proposed control strategy, a DSP-based digital controller is constructed according to the block diagram of Fig. 3.1. The implementation of the proposed control strategy and the corresponding experimental results are given as follows:

A. Implementation of the proposed control strategy

Fig. 3.1 illustrates the block diagram of the speed control system implemented by the proposed robust field weakening control strategy. The q-axis current command is generated from the speed error through a PI speed controller with variable saturation bounds. Thus, the q-axis current command is limited by the bounds which computed from I_{qs} bounds calculator. Two synchronous-frame PI controllers are used to as the d- and q-axis current controllers. A $10\,kHz$ SPWM current-regulated inverter is used as power amplifier which is consisted of a 600 V, 30 A IGBT module, Mitsuibishi CM30MD-12H. The tested 8-pole SMPMSM is Sinano 7CB30-2DE67 whose parameters are shown in Table 2.1. For the loading test of the tested SMPMSM, a permanent magnet DC machine, SEM MT22RS-24, is coupled to the tested SMPMSM. To obtain the information of the rotor, a 2000 pulse/revolution incremental encoder is attached on the shaft of the SMPMSM. For consistency, the dc link voltage, V_{sm} and I_{sm} are chosen to be 100V, 50V and 2A, respectively. Thus, the corresponding ω_{rm}, ω_{rc} and $\omega_{r\ n}$ are found to be 1737, 2060 and 2298 rpm from equations (2.12), (2.13) and (2.16), respectively. To obtain the line current signals, two commercial Hall effect current sensors named LEM LP-55 are used to detect the a- and b-phase current into the signals i_a and i_b, respectively. As shown in Fig 3.6, the signals i_a and i_b are connected to the scaling circuits to generate the signals of i_{as}

and i_{bs}. Actually, the signals of i_{as} and i_{bs} (i.e. the output signals of the scaling circuits shown in Fig 3.7) are to accommodate the input voltage range of the A/D converters in the DSP chip. As shown in Fig 3.7, a low-pass filter circuits are also included in the circuits to reduce the high frequency harmonic effects resulting from the switching of IGBTs.

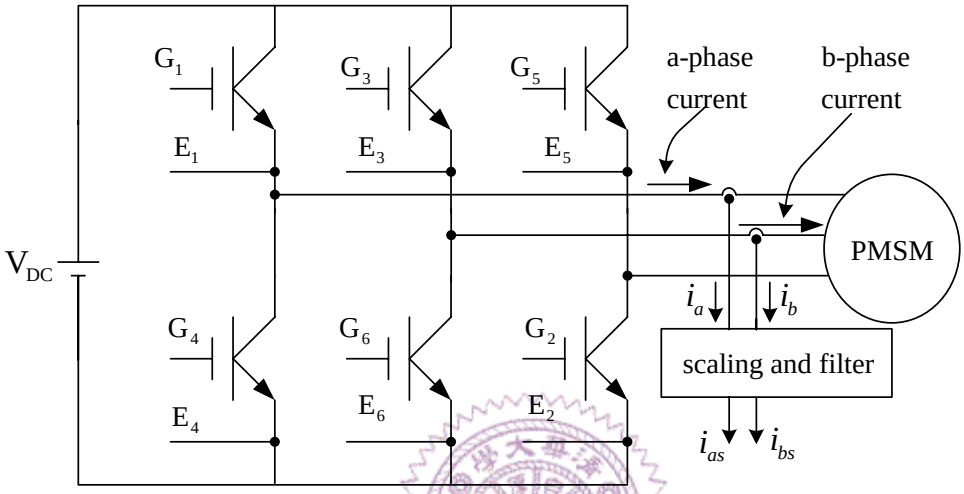

Fig . 3.6. Circuit configuration of the three-phase voltage-source inverter.

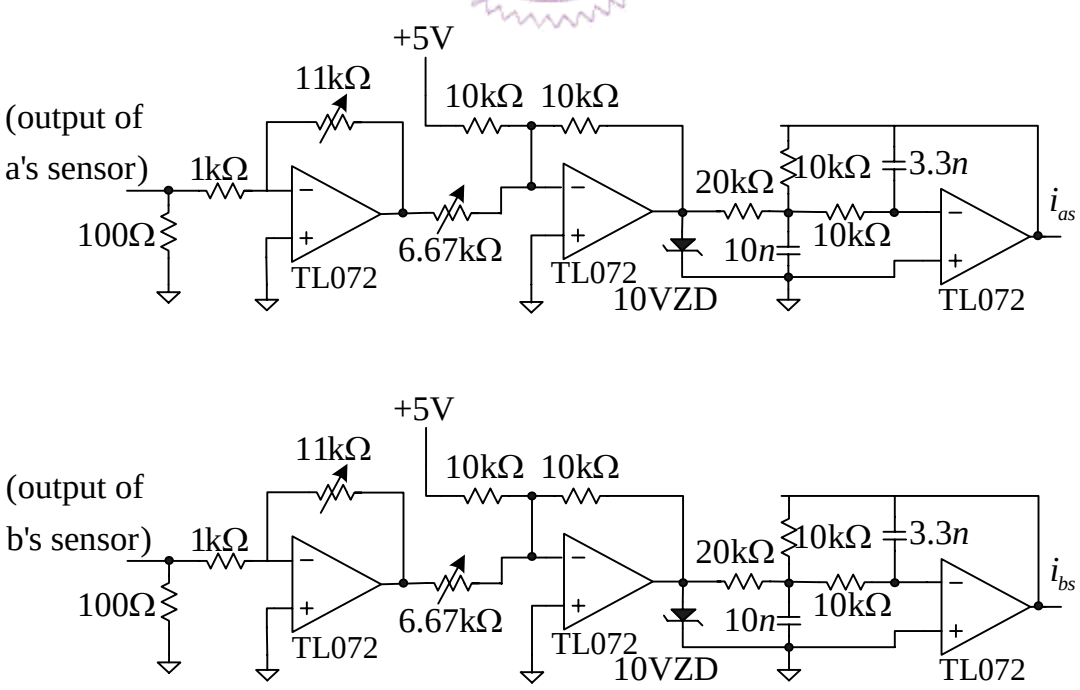

Fig . 3.7. The scaling and filtering circuits of i_{as} and i_{bs}

All the control functions of the drive system shown in Fig 3.1 are implemented fully digital by using a fix-point DSP, TMS320F240, the hardware circuits are greatly simplified. The sampling time period for the PI speed controller with variable-bounds is chosen to be 1.0 ms. Due to the slow change of rotor speed compared with the dynamics of the current loop, the upper and lower I_{qs} bounds calculator also share the same sampling period. However, the sampling time period of the robust tuner and the minimum copper loss controller share the sampling time period as that of the current controller, namely 0.1ms. For the real-time control algorithm, a main program and two periodic interrupts are set in the structure of the DSP program, as shown in Fig 3.8. One fast periodic interrupt with 0.1 ms performs the synchronous sampling of A/D converters, current controller, and calculation of robust tuner, voltage limiter and generation of SPWM. The A/D converters are adopted to convert the phase current signals i_{as} and i_{bs} into digital data (or dc link voltage signal if (3.7) is used to adjust the V_{smv}). To reduce the low frequency harmonics, a phase-invariable voltage limiter will be adopted when the voltage command exceeds the maximum voltage capability, namely $\frac{V_{dc}}{2}$. Another periodic interrupt with 1 ms performs the reading of the information of encoder, calculation of rotor speed, calculation of PI speed controller with variable bounds antiwindup, minimum copper loss control and upper/lower I_{qs} bounds calculation. Besides, a main program is used to initialize the utilized variables, set control registers, enable interrupt functions and transfer the monitored values to D/A converters. Fig 3.8 shows the software configuration in the DSP controller.

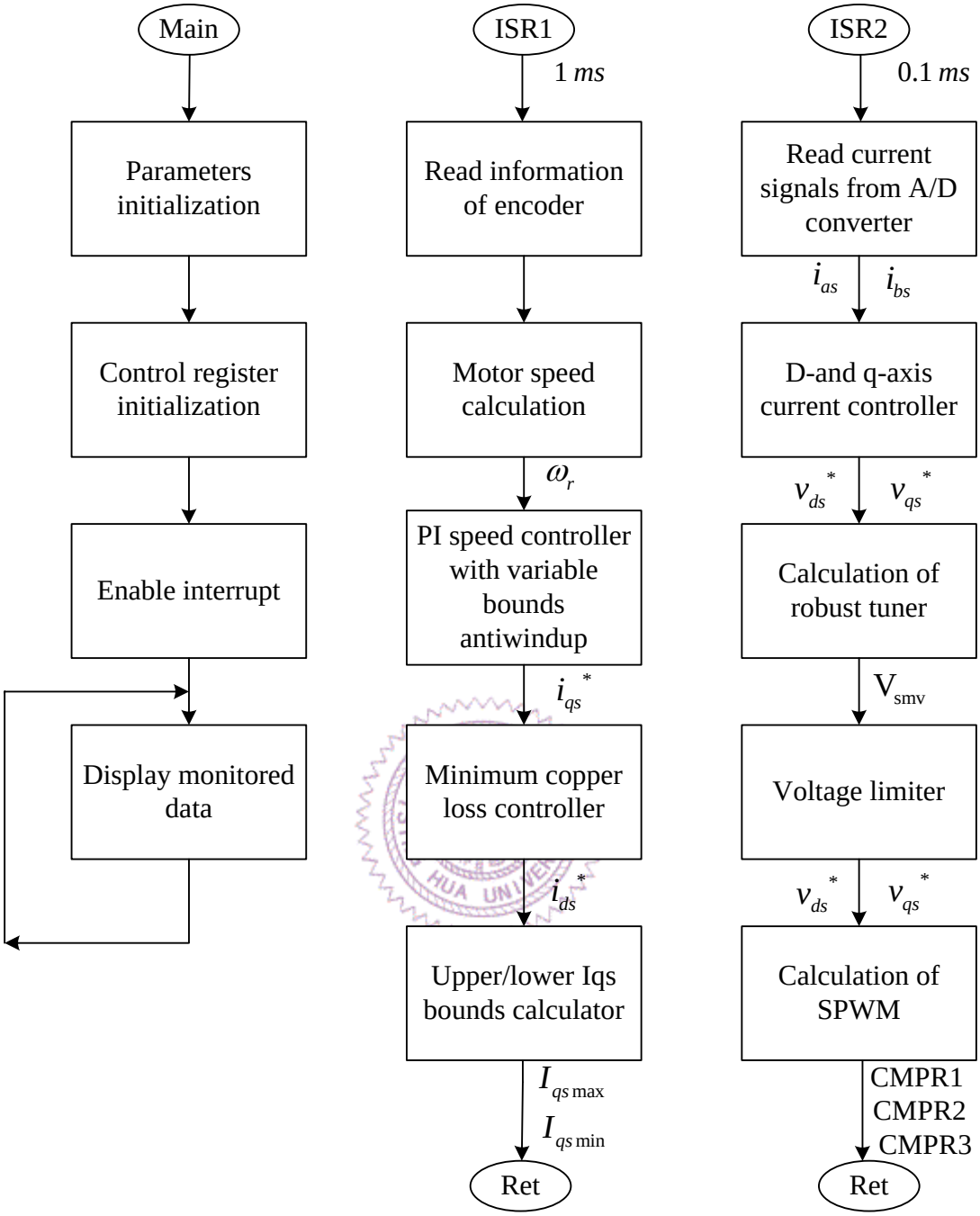

Fig . 3.8. The software configuration in the DSP controller.

B. **Experimental Results**

Several experimental results are provided below to show the characteristics of the proposed control strategy and to compare experimental results with simulation results presented in the previous section. First, to demonstrate the smooth and automatic field

weakening control capability of the proposed control for four-quadrant operation, Fig. 3.9 shows the responses of ω_r , i_{qs} , $I_{qs\max}$ and $I_{qs\min}$ for a periodic step change of speed command from -2400 rpm to +2400 rpm and then back to -2400 rpm. Each speed command is fixed for 1.5 sec. As the description in the section 2.4, the smooth transient between the different operating modes and automatic field weakening control effect can all be observed from Fig. 3.9.

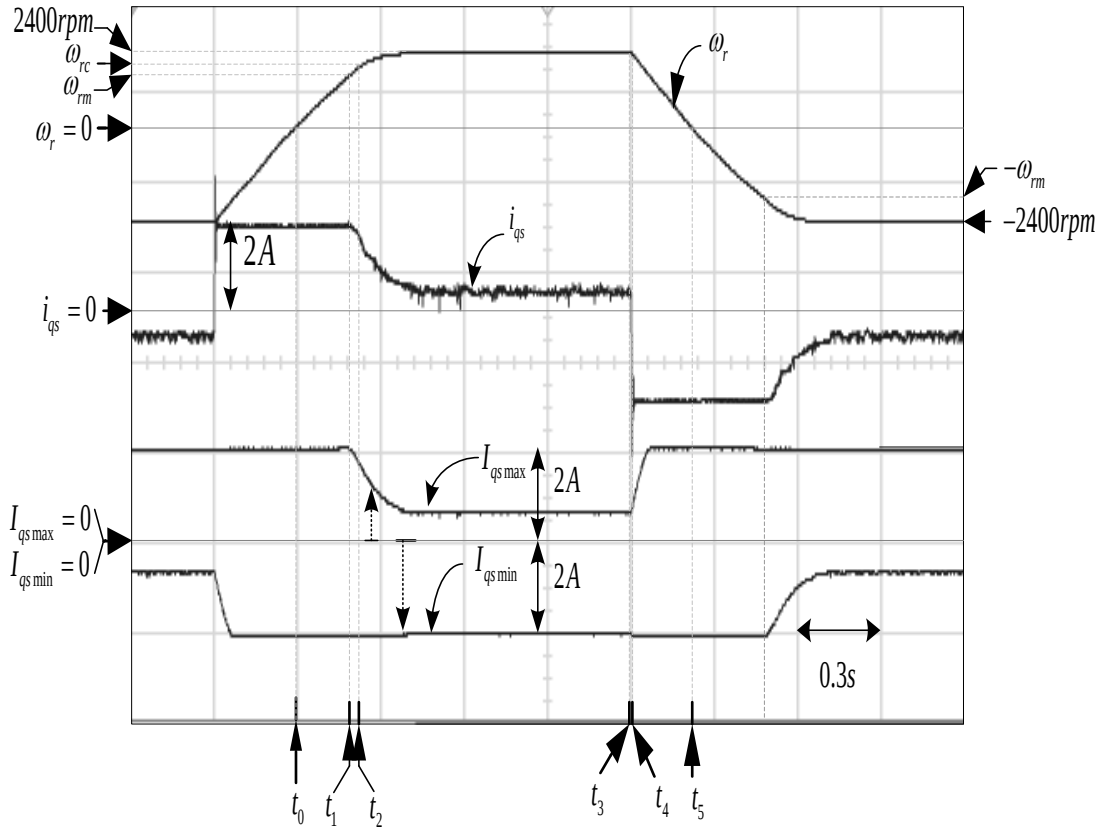

Fig. 3.9. Measured trajectories of ω_r , i_{qs} , and I_{qs} bounds for the proposed control strategy operated in four-quadrant operation.

Next, as an illustration of the partial field weakening control concept, Fig. 3.10 shows the stator current trajectories on the $i_{ds} - i_{qs}$ plane for the heavy and light load conditions. The motor is started from rest and accelerates to the same command of

1950 rpm. Fig. 3.10(a) corresponds to a heavy load of 0.52 Nm approximately. It is seen that the resulting steady state control is the conventional field weakening control $(i_{ds} < 0)$. In contrast, Fig 3.10(b) corresponds to a light load of 0.265 Nm approximately and the resulting steady state control is the conventional constant torque limit control $(i_{ds} = 0)$.

Third, other experiments for illustrating the robust characteristic of the proposed control strategy is considered due to the variation of the dc link voltage (V_{dc}). The motor is started from rest at t_0 up to 2400 rpm. The dc link voltage is subjected to a periodic step change of 15 V for each 1.5 sec and the design of the controller is based on the nominal values shown in Table 2.1. Fig. 3.11(a) shows the corresponding trajectories of V_{dc} , V_{smv} , i_{ds} and i_{qs} respectively and Fig. 3.11(b) shows the corresponding trajectories of $|v_{dq}*|$, i_{du} and $|i_{dq}|^2 = (i_{ds}{}^2 + i_{qs}{}^2)$ which is proportional to copper loss. From Fig. 3.11(a) one can see that V_{smv} can indeed track the variation of V_{dc} for $t > t_1$ in the field weakening regions. After starting transient, the i_{qs} remains constant without the influence of the V_{dc} variations and the resulting speed is kept constant as well (not shown in the figure). As V_{smv} changes, the i_{ds} will also track the variation of V_{dc} according to (3.9) to achieve minimum copper loss. From Figs. 3.12(a) and 3.12(b), in the case of $i_{ds} = 0$ $(t \in [t_3, t_4])$ or in the case of $i_{ds} < 0$ and $|v_{dq}{}^*| = V_{cm}$ $(t \in [t_2, t_3]$ *and* $t \in [t_4, t_5])$, the objective of minimum copper loss control can be achieved. In the above experiment, V_{dc} is directly measured. As a comparison, another experiment under the same conditions but without measuring V_{dc} is also repeated. The corresponding V_{smv} is obtained from (3.8) by using the feedback adjustment. From Fig. 3.12(a) one can see that the convergent rate of V_{smv} and i_{ds} becomes slower as compared with that of Fig. 3.11(a). However, the same

correct results can still be obtained under steady state, which can be checked from Fig. 3.12(b). In other words, one can still achieve the minimum copper loss control under the varying V_{dc} condition.

Fourth, another experiment for illustrating the robust characteristic of the proposed control strategy is considered due to variation of parameters of the SMPMSM. The motor is started from rest at t_0 up to 2100 rpm. The V_{dc} is kept at 100 V and the design of the controller is based on $R_s = 2.36\ \Omega$, $L_s = 7.4\ mH$ and $\lambda_f = 0.07237\ V/(rad/\sec)$, where $|\Delta R_s| = 33.3\%$, $|\Delta L_s| = 25\%$ and $|\Delta \lambda_f| = 25\%$, respectively, when comparing with the nominal values shown in Table 2.1.

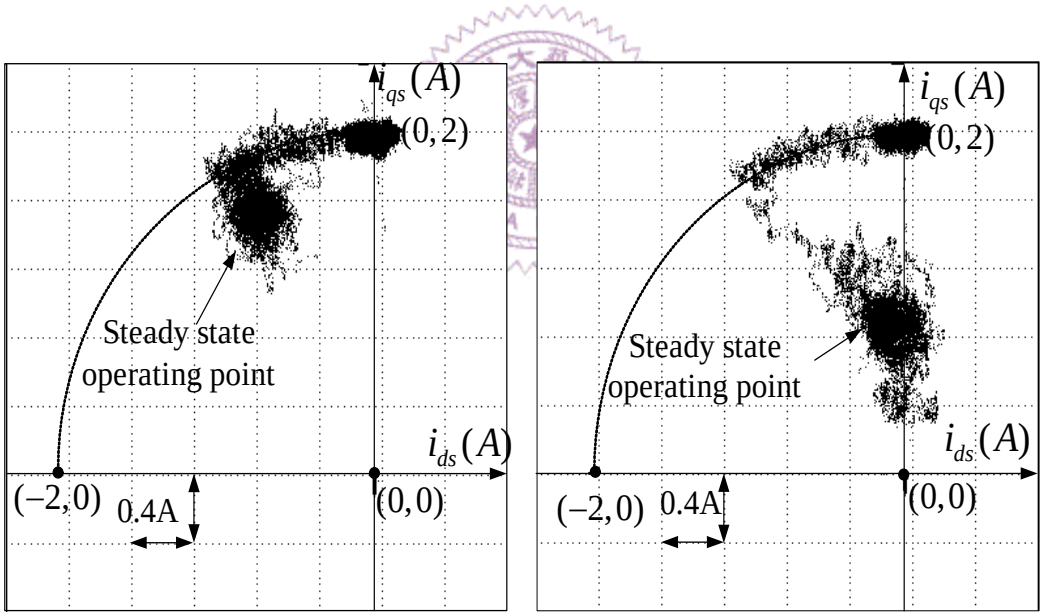

(a) (b)

Fig. 3.10. The $i_{ds} - i_{qs}$ trajectory in the partial field weakening region (a) under heavy load; (b) under light load.

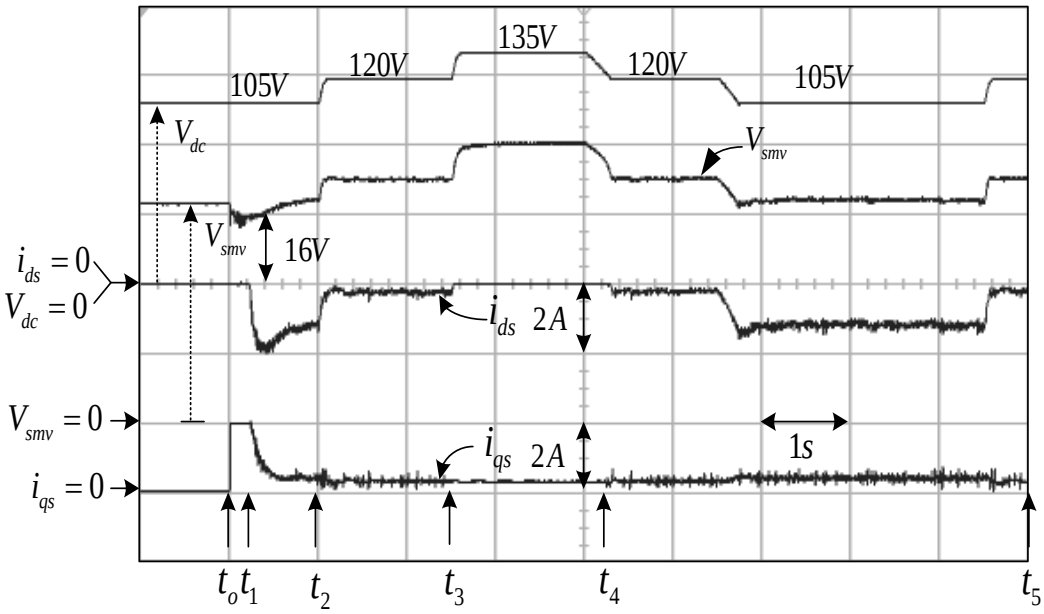

(a)

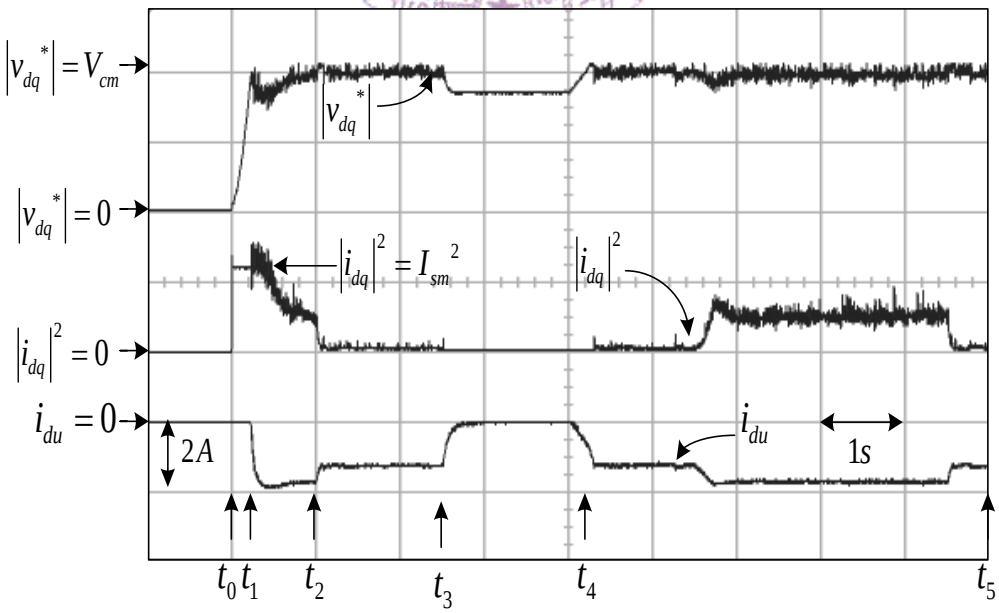

(b)

Fig. 3.11. Trajectories of (a) V_{dc}, V_{smv}, i_{ds} and i_{qs}; (b) $|v_{dq}^*|, |i_{dq}|^2$ and i_{du}, due to variation of V_{dc} and with V_{dc} sensor.

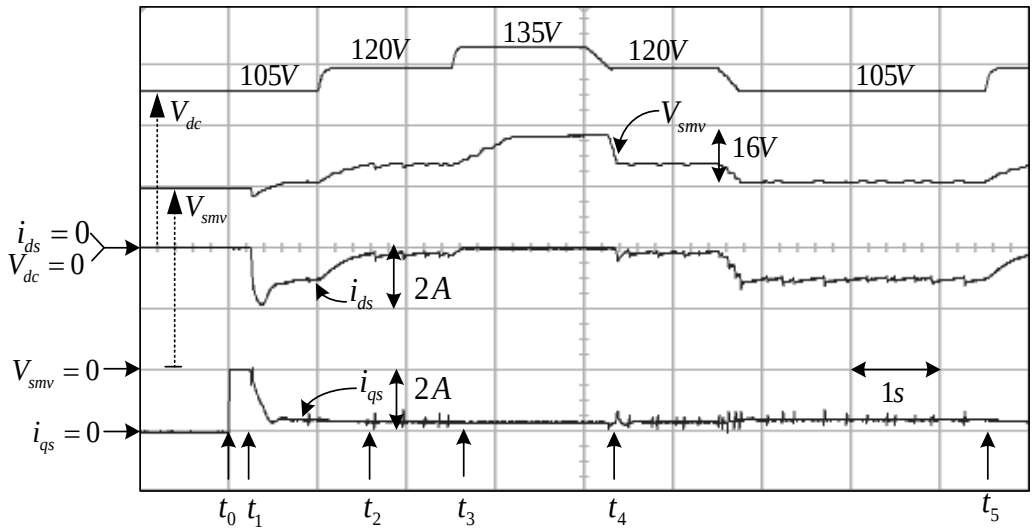

(a)

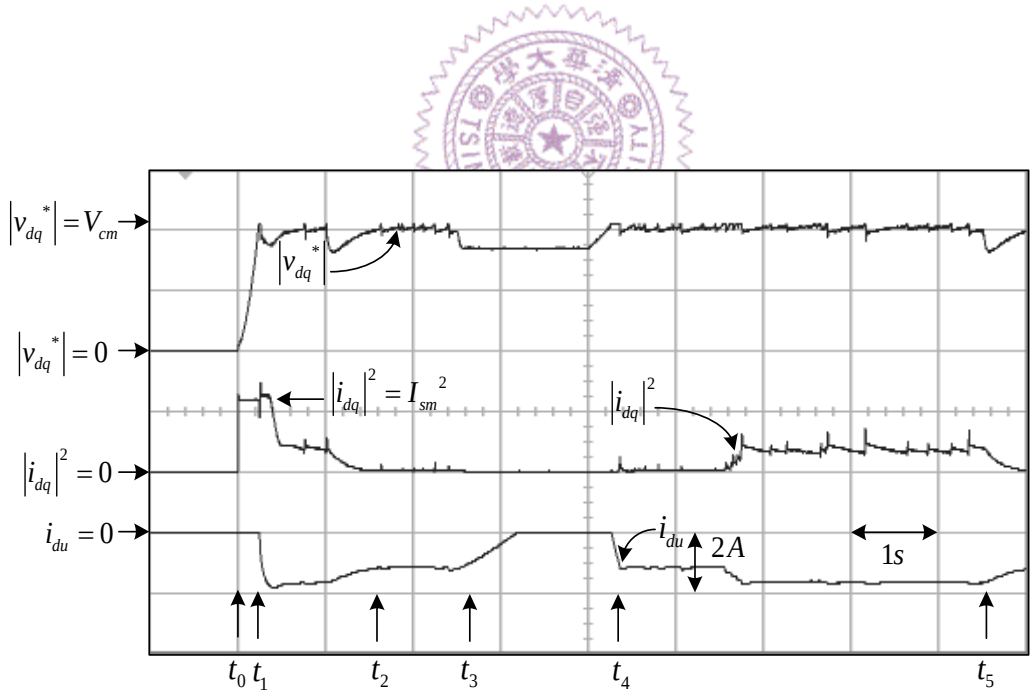

(b)

Fig. 3.12. Trajectories of (a)V_{dc}, V_{smv}, i_{ds} and i_{qs}; (b) $|v_{dq}^*|, |i_{dq}|^2$ and i_{du}, due to variation of V_{dc} and without V_{dc} sensor.

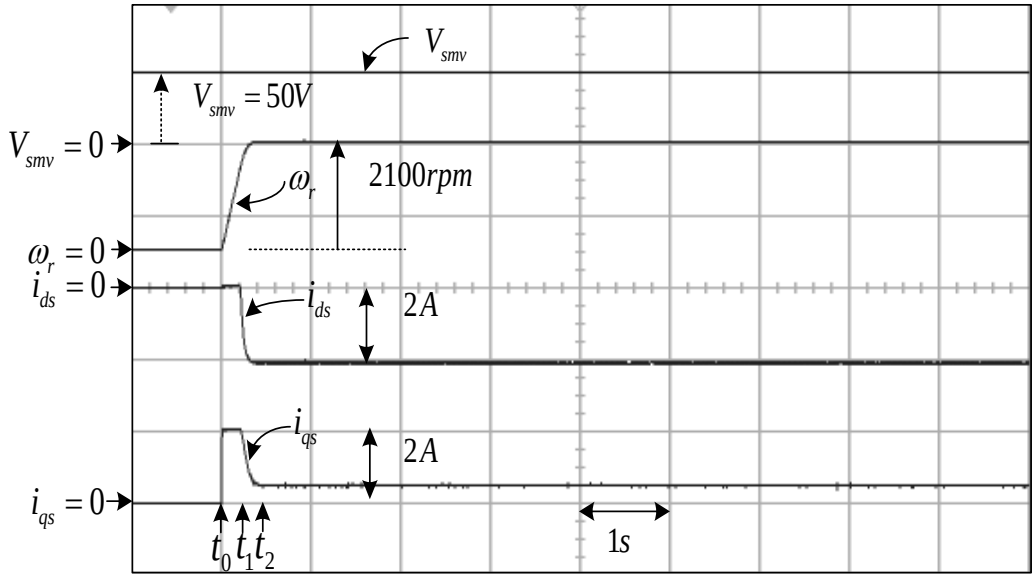

(a)

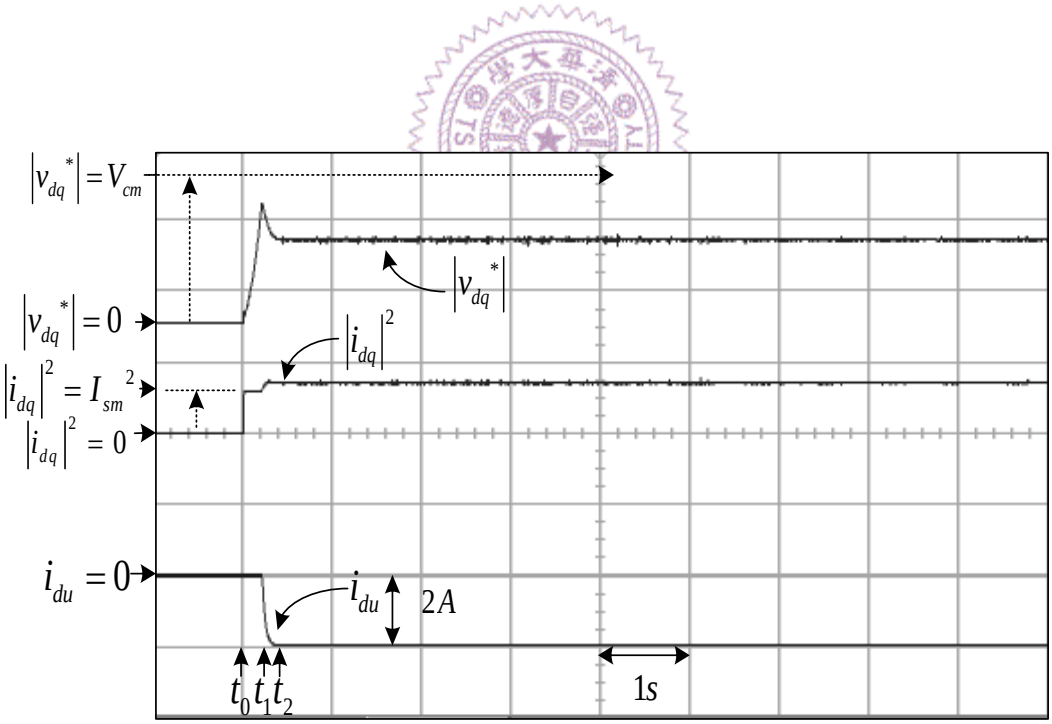

(b)

Fig. 3.13. Experimental results of (a) V_{smv}, ω_r, i_{ds} and i_{qs}; (b) $|v_{dq}^*|$, $|i_{dq}|^2$ and i_{du}, with the robust tuner disabled.

In order to demonstrate the effects of the proposed robust tuner, Fig. 3.13 shows the corresponding measured results with the robust tuner disabled ($K_I = 0$) and Fig. 3.14 shows the corresponding results with the robust tuner enabled. From Figs. 3.13(a) and 3.13(b) one can see that, under the steady state of i_{qs}, i_{ds} is less than zero for $t > t_2$ but $|v_{dq}^*|$ is not equal to V_{cm}. In other words, the maximum available voltage V_{sm} is not applied and the minimum copper loss control is not achieved. On the other hand, Fig. 3.14 shows the corresponding results with the robust tuner enabled. As shown in Figs. 3.14(a) and 3.14(b), the drive is operated in field weakening region ($i_{du} < 0$) for $t > t_1$ and V_{smv} starts to tune according to (3.8). As $|v_{dq}^*|$ approaches V_{cm}, $|i_{dq}|^2$ also decreases. The drive is then operated under minimum copper loss control for $t > t_2$ where $i_{ds} < 0$ and $|v_{dq}^*| = V_{cm}$. In practice, it is rather difficult to keep $|v_{dq}^*|$ exactly equal to V_{cm} due to high gain of the current loop. Therefore, the robust tuner of (3.8) will result in some ripples in V_{smv}, i_{ds}, $|v_{dq}^*|$ and $|i_{dq}|^2$ as can be observed from Figs. 3.11 to 3.14. Fortunately, i_{qs} is not affected significantly as can be seen from Figs. 3.11 to 3.14. Hence the developed torque (T_e) and speed (ω_r) responses can still maintain rather good performance. From the above experiments, one can see that the proposed control can indeed achieve the minimum copper loss in spite of the variations of the dc link voltage and the parameters of the SMPMSM.

Although the parameters of the tested SMPMSM are not ensured to be the same as that in Table 2.1, one can see that the automatic field weakening control, smooth transient of four-quadrant operation, fast speed dynamics and robust minimum copper loss control all can be achieved by the proposed control strategy, as observed from the

results of simulation and experimental measurement.

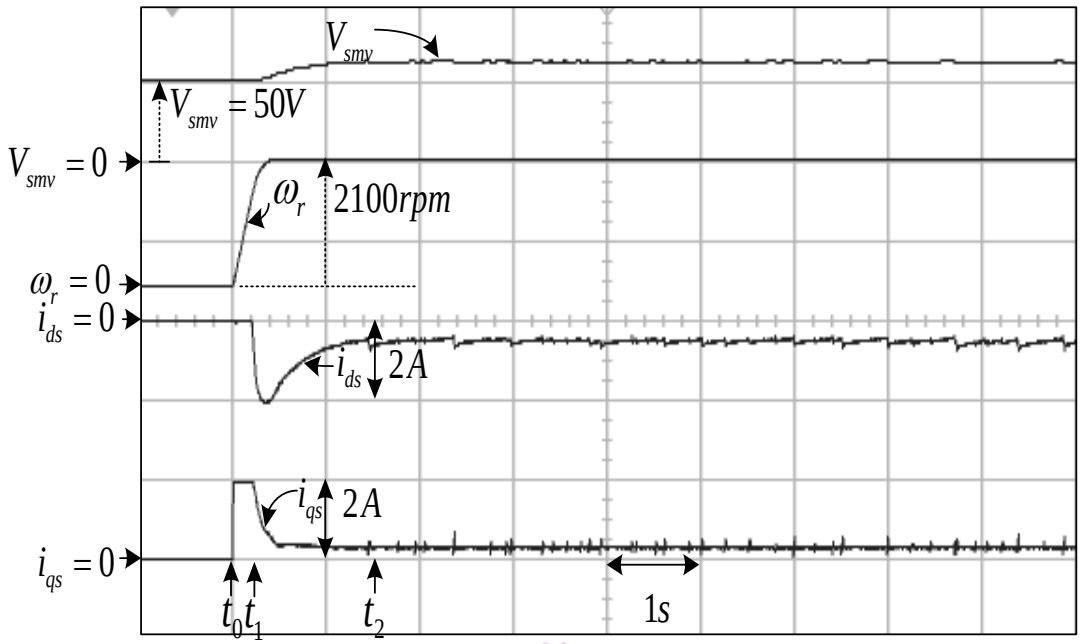

(a)

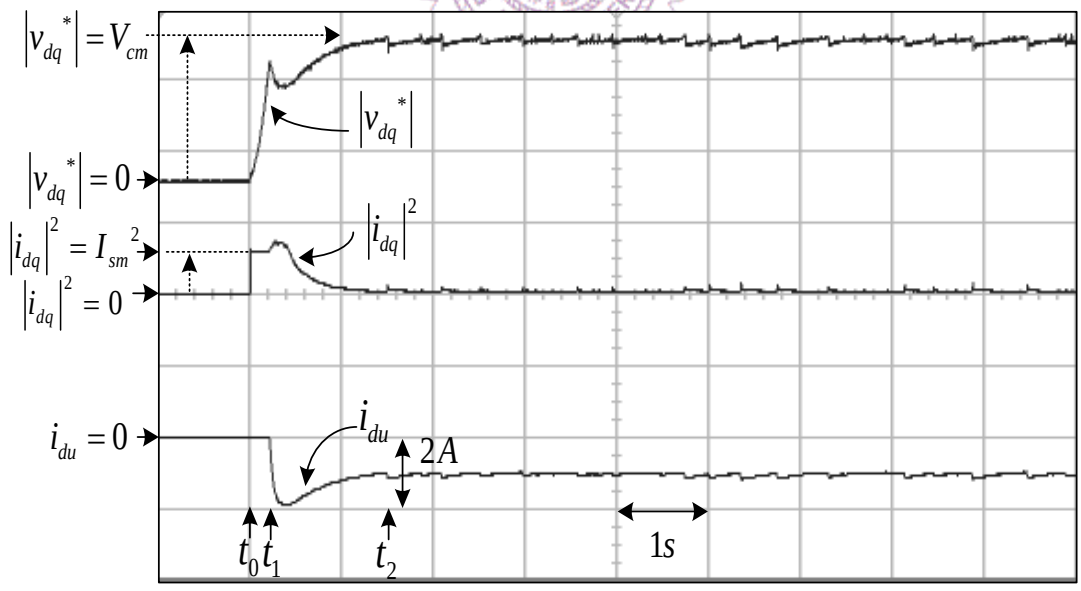

(b)

Fig. 3.14. Experimental results of (a) V_{smv}, ω_r, i_{ds} and i_{qs}; (b) $|v_{dq}^*|$, $|i_{dq}|^2$ and i_{du}, with the robust tuner enabled.